

# Passivation Behavior of Fe-Based Amorphous Coatings Prepared by High-Velocity Air/Oxygen Fuel Processes

H. R. Ma<sup>1,2,3</sup> · J. W. Li<sup>1,2</sup> · C. T. Chang<sup>1,2</sup> · X. M. Wang<sup>1,2</sup> · R. W. Li<sup>1,2</sup>

Submitted: 23 November 2016 / in revised form: 16 July 2017  
© ASM International 2017

**Abstract** Corrosion resistance and passivation behavior of  $\text{Fe}_{63}\text{Cr}_8\text{Mo}_{3.5}\text{Ni}_5\text{P}_{10}\text{B}_4\text{C}_4\text{Si}_{2.5}$  amorphous coatings prepared by the activated combustion high-velocity air fuel (AC-HVAF) and high-velocity oxygen fuel (HVOF) processes have been studied in detail by cyclic potentiodynamic polarization, electrochemical impedance spectroscopy, cathodic polarization and Mott–Schottky approach. The AC-HVAF coating shows higher corrosion resistance than the HVOF coating in 3.5 wt.% NaCl solution, as evidenced by its lower corrosion current density and passive current density. It is found that the superior corrosion resistance of the AC-HVAF coating is attributed to the enhanced formation of a dense passive film with less defective structure, higher pitting resistance and passivity stability, as well as stronger repassivity.

**Keywords** amorphous metals · coatings · corrosion · electrochemical characterization · microstructure

## Introduction

Corrosion is an important issue in numerous industrial applications where it leads to significant loss of energy as well as destructive changes in materials. During the last decades, Fe-based amorphous coatings fabricated using high-velocity oxygen fuel (HVOF) and high-velocity air fuel (HVAF) processes show huge application prospects in the areas involving high corrosion and wear, due to their unique combination of high hardness, good bonding strength, outstanding corrosion and wear resistance (Ref 1–12). Specifically, the SAM2X5 ( $\text{Fe}_{49.7}\text{Cr}_{17.7}\text{Mn}_{1.9}\text{Mo}_{7.4}\text{W}_{1.6}\text{B}_{15.2}\text{C}_{3.8}\text{Si}_{2.4}$  at.%) and SAM1651 ( $\text{Fe}_{48}\text{Mo}_{14}\text{Cr}_{15}\text{Y}_2\text{C}_{15}\text{B}_6$  at.%) amorphous coatings have received extensive attention because of their better performance over others (Ref 1–9). However, the SAM series alloys contain a large amount of Mo ( $\geq 14$  at.%) and/or Cr ( $\geq 15$  at.%), leading to an increase in materials cost.

Recently, we have developed an  $\text{Fe}_{63}\text{Cr}_8\text{Mo}_{3.5}\text{Ni}_5\text{P}_{10}\text{B}_4\text{C}_4\text{Si}_{2.5}$  (at.%) amorphous coating by HVOF that exhibits corrosion resistance comparable to the SAM series amorphous coatings despite its very low Cr and Mo content (Ref 13, 14). Moreover, we have found that the  $\text{Fe}_{63}\text{Cr}_8\text{Mo}_{3.5}\text{Ni}_5\text{P}_{10}\text{B}_4\text{C}_4\text{Si}_{2.5}$  amorphous coating fabricated by activated combustion high-velocity air fuel (AC-HVAF) shows superior wear resistance than that fabricated by HVOF during dry sliding conditions (Ref 15). Some studies demonstrated that the HVAF amorphous coatings possess better corrosion resistance than the HVOF amorphous coatings (Ref 2, 6, 10), indicating the superiority of HVAF in making wear- and corrosion-resistant coatings. It is well known that the study of properties of passive films has fundamental and practical importance in understanding the corrosion of metallic materials for industrial applications. It is interesting that passive films formed on the HVAF and

✉ J. W. Li  
lijw@nimte.ac.cn

✉ C. T. Chang  
ctchang@nimte.ac.cn

<sup>1</sup> Key Laboratory of Magnetic Materials and Devices, Ningbo Institute of Materials Technology and Engineering, Chinese Academy of Sciences, Ningbo 315201, Zhejiang, China

<sup>2</sup> Zhejiang Province Key Laboratory of Magnetic Materials and Application Technology, Ningbo Institute of Materials Technology and Engineering, Chinese Academy of Sciences, Ningbo 315201, Zhejiang, China

<sup>3</sup> Laboratory for Microstructures, Shanghai University, Shanghai 200444, China

HVOF amorphous coatings have almost the same compositions in chloride-containing solutions, even if the corrosion resistance of the amorphous coatings is greatly different (Ref 6). Few reports argued that the superior performance of HVAF amorphous coatings is mainly attributed to the formation of a stable protective film on the etched surfaces (Ref 2, 6).

However, there is still a lack of detailed information concerning comparative evaluation of the properties of passive films formed on Fe-based amorphous coatings prepared by AC-HVAF and HVOF. Therefore, in the present paper an attempt has been made to study the differences of passivation behavior of  $\text{Fe}_{63}\text{Cr}_8\text{Mo}_{3.5}\text{Ni}_5\text{P}_{10}\text{B}_4\text{C}_4\text{Si}_{2.5}$  amorphous coatings sprayed by AC-HVAF and HVOF. We have found that the formation of a dense passive film, with higher pitting resistance and stability as well as stronger repassivity, is responsible for the enhanced corrosion resistance of the AC-HVAF coating, based on the results of the formation, rupture and self-repairing of the passive films.

## Experimental Procedures

In the present work, the mild steel with a dimension of  $20\text{ mm} \times 20\text{ mm} \times 3\text{ mm}$  was used as substrate. All substrates were polished and degreased by ethanol, dried in air and then grit-blasted prior to thermal spraying.  $\text{Fe}_{63}\text{Cr}_8\text{Mo}_{3.5}\text{Ni}_5\text{P}_{10}\text{B}_4\text{C}_4\text{Si}_{2.5}$  powders with sizes in the range of 20–45  $\mu\text{m}$  manufactured by high-pressure argon gas atomization were sieved out as the feedstock powders for spraying. The majority of powders showed good sphericity and a smooth surface with completely amorphous structure (Ref 14, 15). The amorphous coatings were fabricated by AC-HVAF and HVOF thermal spray systems in the open air. (Detailed spraying parameters were presented in Ref 15). The microstructure and morphology of the as-sprayed coatings were characterized by x-ray diffraction using  $\text{Cu K}\alpha$  radiation (XRD, D8 Advance) and field emission scanning electron microscopy (SEM, FEI Quanta FEG 250). The porosity of the coatings was evaluated by analyzing the SEM micrographs with the Image Pro-Plus 6.0 software. The oxidation rate was examined by the oxygen–nitrogen analyzer.

For electrochemical studies, the as-sprayed coatings were electrically connected to copper wires and embedded in epoxy resin so that only the test surfaces remained free. The measurements were performed in 3.5 wt.% NaCl solution open to air at room temperature. An electrochemical workstation (Modulab, Solartron) connected to a cell with three-electrode arrangement with a platinum wire as counter electrode and a saturated calomel electrode (SCE) as reference electrode was employed. Cyclic

potentiodynamic polarization was performed swept from  $-0.6$  to  $1.5\text{ V}$  at a potential sweep rate of  $1.0\text{ mV s}^{-1}$  and then backed to form a hysteresis loop. Electrochemical impedance spectroscopy (EIS) measurements were carried out with a potential amplitude of 10 mV in a frequency ranging from 10 kHz to 0.01 Hz. Current–time transient measurements were performed by immersing coatings at applied polarization potentials of 0.2, 0.4, 0.6 and 0.8 V for 1800 s, respectively. Cathodic polarization measurements were carried out with the constant current of 1 mA. Mott–Schottky plots were determined with a scanning potential range from  $-0.6$  to  $1.2\text{ V}$ , and the measured frequency was 1 kHz. For comparison, the AISI 304 stainless steel (304 SS) was selected to perform the electrochemical measurements in the same way. Each test was repeated three to five times for repeatability and reliability.

## Results

Figure 1(a) displays XRD patterns of the coatings prepared by AC-HVAF and HVOF. The AC-HVAF coating shows only a broad diffraction hump indicating its fully amorphous nature, while the HVOF coating exhibits weak sharp diffraction peaks revealing a very tiny amount of crystalline phases. Figure 2(a) and (b) shows that both coatings show a dense structure with similar thickness of 200  $\mu\text{m}$ . However, some micropores and micro-cracks are distributed in the HVOF coating, for example, the interface of partially melted particle (Fig. 2d). The porosity of the AC-HVAF coating is 0.4%, much lower than that of the HVOF coating (1.5%), as shown in Fig. 1(b). Figure 1(b) also shows the oxygen content of 0.24 wt.% in AC-HVAF coating and 0.12 wt.% in HVOF coating, which are all lower than common values in other literatures (Ref 2). Although the AC-HVAF coating contains more oxygen than the HVOF coating, the oxygen obviously concentrated in dark strip-shaped inclusions in the HVOF coating (the inset in Fig. 2d) (Ref 16), which are only vaguely detected in the AC-HVAF coating (Fig. 2c). Thus, the AC-HVAF coating has a denser microstructure than the HVOF coating. Besides, the difference in microstructure would exert an important influence on corrosion resistance of the coatings.

Figure 3(a) shows the cyclic polarization curves of the amorphous coatings prepared by AC-HVAF and HVOF in 3.5 wt.% NaCl solution. The data of 304 SS are shown for comparison. The electrochemical corrosion parameters obtained from the cyclic polarization curves are listed in Table 1. Compared to the HVOF coating, the AC-HVAF coating exhibits a lower corrosion current density ( $I_{\text{corr}}$ ) and one order reduction in passive current density ( $I_{\text{pass}}$ ), suggesting that the AC-HVAF coating exhibits more

**Fig. 1** (a) XRD patterns and (b) porosity/oxidation content of the AC-HVAF coating and HVOF coating

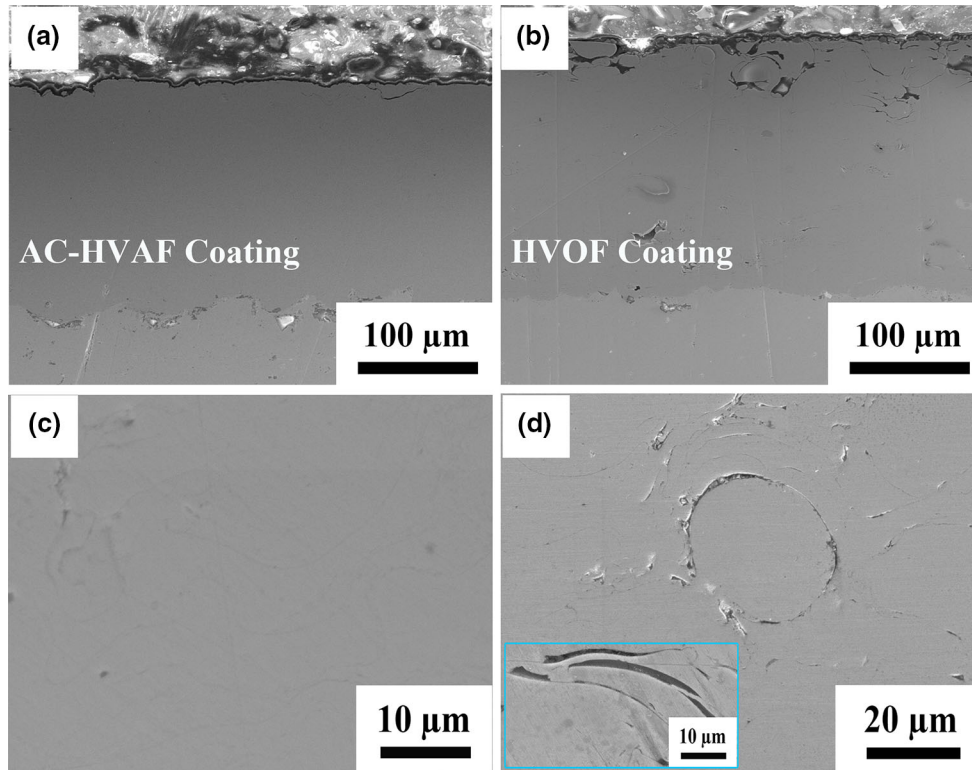
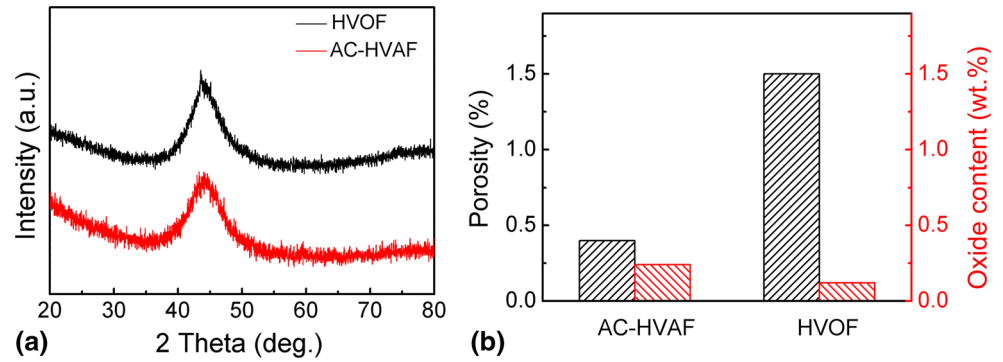


**Fig. 2** SEM micrograph of the (a) AC-HVAF coating and (b) HVOF coating. (c) and (d) are magnified images from (a) and (b), respectively

superior corrosion resistance than the HVOF coating. The 304 SS passivates spontaneously with much lower  $I_{\text{pass}}$  ( $\sim 10^{-6}$  A cm $^{-2}$ ) than the amorphous coatings, which should be related to the negative effects of defective regions on coating matrix (micropores and oxide inclusions, as described in Fig. 2). However, the amorphous coatings can be passivated with much higher transpassive potential ( $E_{\text{tr}} = 1.10$  V) and wider passivation region ( $\sim 1.50$  V) than 304 SS due to the homogeneous single-phase nature of the amorphous coatings (Ref 17, 18). Besides, it can be seen from Fig. 3(a) and Table 1 that repassivation potential ( $E_{\text{rp}}$ , the potential below which pits repassivate) values of the 304 SS, HVOF and AC-HVAF coatings are around  $-0.27$ ,  $0.86$  and  $0.95$  V, respectively.

The higher  $E_{\text{rp}}$  of the AC-HVAF coating indicates a better pitting resistance compared with the 304 SS and HVOF coating (Ref 19).

Figure 3(b), (c), and (d) presents the SEM images of the corroded surfaces of amorphous coatings and 304 SS after potentiodynamic polarization tests. Obvious corrosion pits with various sizes can be found on the corroded surfaces of all samples, indicating that these samples in a chloride-containing solution are governed by a localized pitting corrosion. The insets of Fig. 3(b), (c), and (d) show the magnified images of typical corrosion pits. It can be clearly noted that the average sizes of corrosion pits on amorphous coatings are much smaller than that on 304 SS. However, the number of pits on the HVOF coating is significantly

**Fig. 3** Cyclic polarization curves (a) and SEM images of corroded surface (b, c) of the amorphous coatings prepared by AC-HVAF and HVOF in 3.5 wt.% NaCl solution, respectively. In (a) and (d), data of the AISI 304 stainless steel are shown for comparison

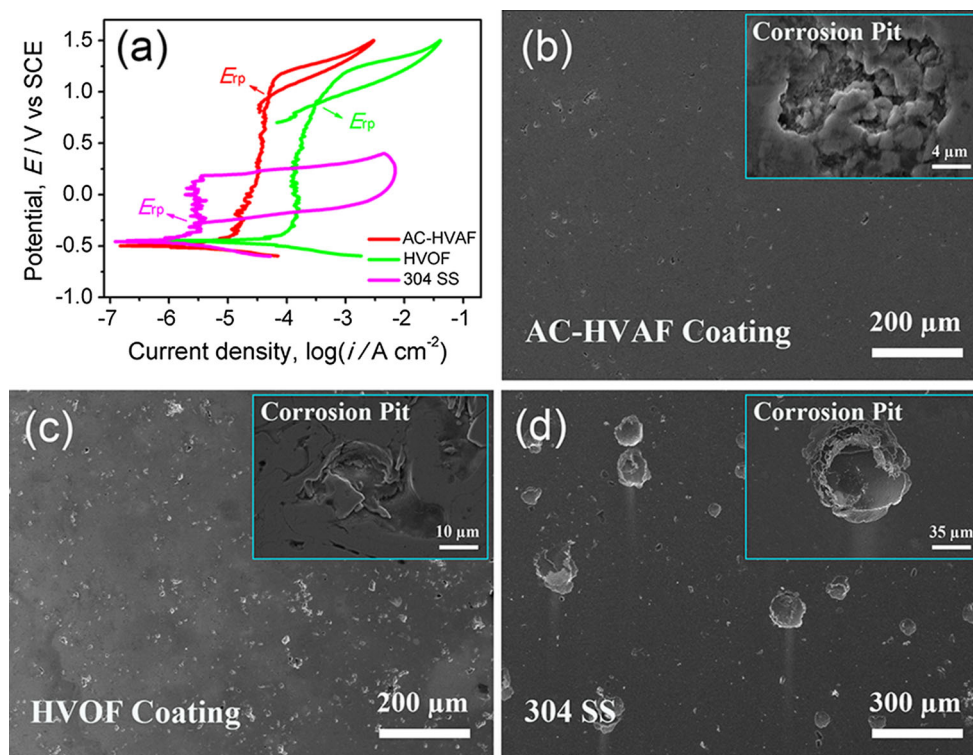


**Table 1** Electrochemical parameters obtained from cyclic polarization curves

	$E_{\text{corr}}$ , V	$I_{\text{corr}}$ , A cm <sup>-2</sup>	$I_{\text{pass}}$ , A cm <sup>-2</sup>	$E_{\text{tr}}$ , V	$E_{\text{rp}}$ , V
AC-HVAF coating	-0.49	$1.8 \times 10^{-6}$	$3.9 \times 10^{-5}$	1.12	0.95
HVOF coating	-0.45	$8.3 \times 10^{-6}$	$1.6 \times 10^{-4}$	1.11	0.86
304 SS	-0.45	$7.6 \times 10^{-7}$	$3.2 \times 10^{-6}$	0.18	-0.27

$E_{\text{corr}}$ ,  $I_{\text{corr}}$ ,  $I_{\text{pass}}$ ,  $E_{\text{tr}}$  and  $E_{\text{rp}}$  represent the corrosion potential, corrosion current density, passive current density, transpassive potential and repassivation potential, respectively

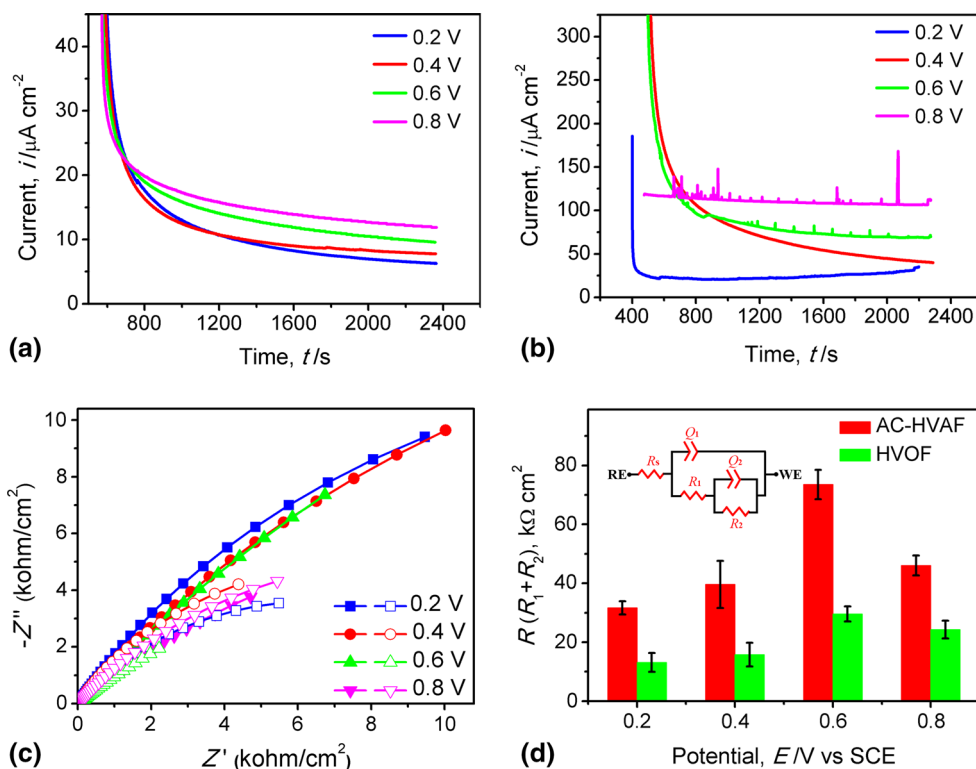
more than that on the AC-HVAF coating, suggesting that pitting is easier to occur on the HVOF coating.

To reveal more details on the pitting behavior, potentiostatic polarization measurements were performed. Figure 4(a) and (b) shows current–time curves of the amorphous coatings in 3.5 wt.% NaCl solution at applied potentials of 0.2, 0.4, 0.6, and 0.8 V (less than  $E_{\text{tr}}$ ). The current density initially moves rapidly toward a more negative value and then reaches a relatively steady value with time due to the initial formation and growth of the passive films formed on the sample surfaces (Ref 20, 21). In addition, the current density values of the AC-HVAF coating are lower than those of the HVOF coating under all applied potentials. Moreover, many sharp current transients can be detected on the HVOF coating at high potentials (Fig. 4b). These current transients are usually derived from metastable corrosion pits induced by local breakdown of the passive film (Ref 22, 23). However, the micro-transients cannot be distinguished in the AC-HVAF coating within the present detection limits (Fig. 4a). These results

demonstrate that the passive film formed on the AC-HVAF coating has better pitting resistance and protection performance than that of the HVOF coating, which agree well with the result of cyclic polarization (Fig. 3a).

Figure 4(c) displays the Nyquist and Bode plots of the amorphous coatings prepared by AC-HVAF and HVOF in 3.5 wt.% NaCl solution at applied potentials of 0.2, 0.4, 0.6 and 0.8 V. It can be seen that the impedance of the AC-HVAF coating is larger than that of the HVOF coating, suggesting that the passive film of the former provides a more effective barrier against corrosive ion. An equivalent circuit,  $R_s R_1 [Q_1 (R_2 Q_2)]$ , is proposed to analyze the impedance data for the amorphous coatings (Ref 24), as shown in the inset of Fig. 4(d).  $R_s$  is the solution resistance,  $Q_1$  represents the capacitance of the passive film, coupled with a resistance  $R_1$  due to the ionic paths through the film, and  $Q_2$  and  $R_2$  associate with the capacitance and the charge-transfer resistance at the interfaces of electrolyte/passive film/metal, respectively. Figure 4(d) shows the applied potential dependence of the total resistance ( $R_1 + R_2$ )

**Fig. 4** Current–time curves of the (a) AC-HVAF and (b) HVOF coatings at applied potentials of 0.2, 0.4, 0.6 and 0.8 V, respectively. (c) Nyquist plots of the AC-HVAF (solid) and HVOF (hollow) coatings at applied potentials of 0.2, 0.4, 0.6 and 0.8 V, respectively. (d) Total resistance for ion transfer ( $R_1 + R_2$ ) as a function of the applied potential for the AC-HVAF and HVOF coatings; the inset is equivalent circuit for fitting the impedance spectra



obtained from the equivalent circuit. Although the trend of the total resistance with applied potential is similar for both coatings, the total resistance of the AC-HVAF coating is larger than that of the HVOF coating, leading to the lower current density values of the AC-HVAF coating during potentiostatic polarization measurements, as shown in Fig. 4(a) and (b).

Figure 5(a) presents the time evolution of the potential for the amorphous coatings during cathodic polarization measurements. Both curves increase rapidly at the beginning, representing continuous growth of passive oxide films, and then become flat and stable with time. Compared to the HVOF coating, the potential of the AC-HVAF coating increases to more positive value and the time taken to reach a stationary potential is reduced. A shorter time to reach a stable value is related to a faster growth rate of passive film formed on the AC-HVAF coating (Ref 25). Higher stationary potential is indicative of thickening of the passive film formed on the AC-HVAF coating or more compactness and stability of the passive film (Ref 26).

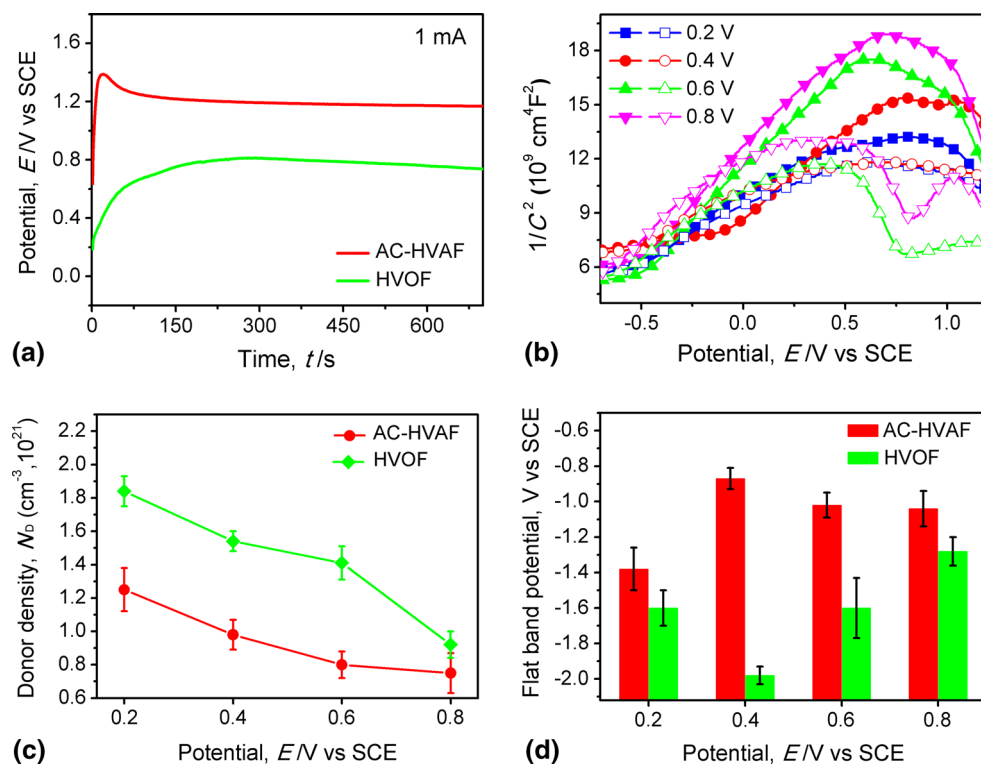
To further understand the structural characteristic of the passive film, Mott–Schottky (MS) analysis based on the measurement of apparent capacitance as a function of potential was carried out. Figure 5(b) shows the MS plots for the passive films formed in 3.5 wt.% NaCl solution at applied potentials of 0.2, 0.4, 0.6 and 0.8 V. The MS plots have positive slopes at the initial stage, indicating that the passive films show n-type semiconductor character. With

increasing potential, the electronic properties of the passive films change from n-type to p-type, suggesting the initiation of transpassive dissolution (Ref 27). However, the critical potential ( $\sim 0.75$  V) of the AC-HVAF coating is higher than that ( $\sim 0.6$  V) of the HVOF coating, revealing that the AC-HVAF coating shows higher stable passivity.

According to the point defect model, the major carrier species in n-type oxide films are oxygen vacancies (donors) generated at the metal/film interface, which contribute to the formation and breakdown of the passive film (Ref 28, 29). Thus, the donor density ( $N_D$ ) has a great influence on the stability of the passive films. The variation of  $N_D$  as a function of potential is presented in Fig. 5(c). Detailed calculation method of  $N_D$  can be found in Ref 23. It is clear that the  $N_D$  values of both coatings decrease with increasing passivated potential, but the AC-HVAF coating exhibits lower  $N_D$  than the HVOF coating, suggesting a more compact and stable passive film formed on the AC-HVAF coating. This result is in good accordance with other electrochemical test outcomes.

Figure 5(d) displays the flat-band potentials of the passive films obtained from MS plots (Ref 30). When the applied potential is more positive than the flat-band potential, the upward band bending will become higher. In this case, it is easier for corrosive anions to intrude into the n-type semiconductor film and finally result in pitting (Ref 31). As shown in Fig. 4(d), the flat-band potentials of the AC-HVAF coating are higher than those of the HVOF

**Fig. 5** (a) Potential–time curves during cathodic polarization for the AC-HVAF and HVOF coatings. (b) Mott–Schottky plots of the passive films formed on the AC-HVAF (solid) and HVOF (hollow) coatings at applied potentials of 0.2, 0.4, 0.6 and 0.8 V, respectively. (c) and (d) are donor density ( $N_D$ ) and flat-band potentials calculated from the slopes of Mott–Schottky plots, respectively



coating under the same applied potentials, indicating that the localized corrosion occurring on the HVOF coating is more severe compared to the AC-HVAF coating. The analysis can be confirmed from previous surface topography observations.

## Discussion

A metal surface is generally separated from oxygen and corrosive ions in nature due to coverage by a protective oxide film, and thus, further corrosion is relatively slow. This is called spontaneous passivity. The ability to resist corrosion depends on the formation, rupture (depassivation) and self-repairing (repassivation) of the passive film formed on the material's surface (Ref 17, 32). Therefore, to explain why the corrosion resistance of the AC-HVAF coating is superior to that of the HVOF coating in 3.5 wt.% NaCl solution, it is reasonable to study the differences of the passive film characteristics of these two coatings, as discussed below:

1. Formation of the passive film: The growth of the passive film on the AC-HVAF coating is faster than that on the HVOF coating (Fig. 5a). Besides, the electronic character is a key factor that can influence the properties of passive films with the same compositions. The higher the donor density, the better the conductivity of the passive film (Ref 21, 33). The

donor density values of the passive films of the HVOF coating are higher than those of the AC-HVAF coating (Fig. 5c). This implies an easier oxygen and chloride ions transport to the passive film formed on the HVOF coating, which could be further proved by its lower total charge-transfer resistance (Fig. 4d) and higher current density during potentiostatic polarization (Fig. 4a and b). In general, passive films are easily formed on amorphous alloys with homogeneous single-phase nature, due to a rapid dissolution of less noble elements and fast accumulation of passivation elements (Ref 18, 34). As shown in Fig. 2, heterogeneous phases and slightly crystallization in the HVOF coating would have a negative impact on its structural homogeneities. Therefore, it is reasonable that the passive film formed on the AC-HVAF coating has a higher growth rate and more compact property than the HVOF coating. In this view, the faster formation of a passive film with fewer defects on the AC-HVAF coating provides greater protective ability to obstruct the permeation of aggressive ions into the oxide film.

2. Rupture of the passive film: The breakdown of passive film on a metal surface is proposed to be caused by pitting corrosion or localized ruptures (Ref 35, 36). In contrast to the HVOF coating, the AC-HVAF coating exhibits less number of current micro-transients (Fig. 4a and b) and microscale pit events during corrosion process (Fig. 3b and c), indicating that pit

initiation is inhibited greatly on the AC-HVAF coating. There are much more micropores and micro-cracks dispersed in the HVOF coating, which can be permeated by corrosive medium accelerating the initiation of pits. Continuous dissolution can make disconnected pores expand and interconnect, and eventually to form big gaps destroying the completeness of the passive film (Ref 9). On the other hand, the galvanic effect between the Cr-depleted and the Cr-rich zone at the edge of the intersplat regions can also lead to the pitting initiation in Fe-based amorphous coatings (Ref 3). Therefore, the HVOF coating with more distinct oxide inclusions is more prone to pitting events. Moreover, the donor density of passive film on the HVOF coating is higher than that on the AC-HVAF coating, implying that the former is more susceptible to pitting corrosion (Ref 21). In addition, the relatively lower transpassive dissolution and flat-band potentials of the HVOF coating make aggressive anions invade the oxide film easier, resulting in more severe localized dissolution (Fig. 5). These results illustrate that the HVOF coating has more defects such as micropores/micro-cracks and oxide inclusions as preferred sites for pitting nucleation and growth, and the AC-HVAF coating exhibits better passivity stability than the HVOF coating.

3. Self-repairing of the passive film: When the passive film is broken by the attack of corrosive environments, corrosive dissolution and/or rusting of materials will be promoted. If the film-broken surface is repaired (repassivation), corrosive damage of the metal can be prevented (Ref 33). Thus, self-repairing ability of the passive film is also important for corrosion resistance of metals. The passivation self-repairing process is easier to occur in the AC-HVAF coating than in the HVOF coating, as proved by cyclic polarization tests (Fig. 3a). Generally, fresh corrosion pits will be inactive after short time of growth and then repassivate, because a steady salt layer formed on the bottom of the pit leads to a sharp decrease in the local current density which is too low to sustain the aggressive solution (and low pH) around the pit (Ref 36–38). Structural inhomogeneity can cause aggressive local environment near the oxides/electrolyte surface resulting from a local acidification and a condensation of chloride ions, which contributes to the formation and growth of corrosion pits (Ref 22, 39). On the other hand, the fully amorphous structure of the AC-HVAF coating is beneficial for inducing a less defective oxide/metal interfacial region to resist pit propagation (Ref 22). Therefore, the precursor shallow pits formed on the AC-HVAF coating will repassivate easier than those on the HVOF coating, as shown in Fig. 3.

## Conclusions

The structure, corrosion resistance and passivation behavior of the  $\text{Fe}_{63}\text{Cr}_8\text{Mo}_{3.5}\text{Ni}_5\text{P}_{10}\text{B}_4\text{C}_4\text{Si}_{2.5}$  amorphous coatings prepared by AC-HVAF and HVOF have been investigated. The AC-HVAF coating exhibits lower corrosion current density and passive current density than the HVOF coating in 3.5 wt.% NaCl solution. Compared to the HVOF coating, the faster formation of a passive film with fewer defects on the AC-HVAF coating can provide greater protection performance against corrosive ions. Besides, the passive film formed on the AC-HVAF coating exhibits higher pitting resistance and passivity stability than the HVOF coating. Moreover, the passive film formed on the AC-HVAF coating can be easier repassivated than that on the HVOF coating, indicating a stronger self-repairing ability of the former. Therefore, the AC-HVAF coating with a compact and fully amorphous structure is good for the formation of a denser passive film with higher pitting resistance and stability as well as stronger repassivity, leading to better corrosion resistance than the HVOF coating.

**Acknowledgments** Financial support is from National Natural Science Foundation of China (Grant Nos. 51501210 and 51571207) and Ningbo Municipal Nature Science Foundation (Grant No. 2017A610034). The authors would like to thank J. Shen and H. Li for technical assistance.

## References

1. J. Farmer, J.S. Choi, C. Saw, J. Haslam, D. Day, and P. Hailey, Iron-Based Amorphous Metals: High-Performance Corrosion-Resistant Material Development, *Metall. Mater. Trans. A*, 2009, **40**, p 1289–1305
2. R.Q. Guo, C. Zhang, Q. Chen, Y. Yang, N. Li, and L. Liu, Study of Structure and Corrosion Resistance of Fe-Based Amorphous Coatings Prepared by HVAF and HVOF, *Corros. Sci.*, 2011, **53**, p 2351–2356
3. C. Zhang, K.C. Chan, Y. Wu, and L. Liu, Pitting Initiation in Fe-Based Amorphous Coatings, *Acta Mater.*, 2012, **60**, p 4152–4159
4. Z.B. Zheng, Y.G. Zheng, W.H. Sun, and J.Q. Wang, Effect of Applied Potential on Passivation and Erosion–Corrosion of a Fe-Based Amorphous Metallic Coating Under Slurry Impingement, *Corros. Sci.*, 2014, **82**, p 115–124
5. W.M. Guo, Y.P. Wu, J.F. Zhang, S. Hong, G.Y. Li, G.B. Ying, J. Guo, and Y.J. Qin, Fabrication and Characterization of Thermal-Sprayed Fe-Based Amorphous/Nanocrystalline Composite Coatings: An Overview, *J. Therm. Spray. Technol.*, 2014, **23**, p 1157–1180
6. Y. Wang, Z.Z. Xing, Q. Luo, A. Rahman, J. Jiao, S.J. Qu, Y.G. Zheng, and J. Shen, Corrosion and Erosion–Corrosion Behaviour of Activated Combustion High-Velocity Air Fuel Sprayed Fe-Based Amorphous Coatings in Chloride-Containing Solutions, *Corros. Sci.*, 2015, **98**, p 339–353
7. M. Yasir, C. Zhang, W. Wang, Z.W. Zhang, and L. Liu, Tribocorrosion Behavior of Fe-Based Amorphous Composite Coating

- Reinforced by Al<sub>2</sub>O<sub>3</sub> in 3.5% NaCl Solution, *J. Therm. Spray. Technol.*, 2016, **25**, p 1554-1560
8. P. Xu, C. Zhang, W. Wang, and L. Liu, Pitting Mechanism in a Stainless Steel-Reinforced Fe-Based Amorphous Coating, *Electrochim. Acta*, 2016, **206**, p 61-69
  9. S.D. Zhang, J. Wu, W.B. Qi, and J.Q. Wang, Effect of Porosity Defects on the Long-Term Corrosion Behaviour of Fe-Based Amorphous Alloy Coated Mild Steel, *Corros. Sci.*, 2016, **110**, p 57-70
  10. E. Sadeghimeresht, N. Markocsan, and P. Nylén, Microstructural Characteristics and Corrosion Behavior of HVOF- and HVOF-Sprayed Fe-Based Coatings, *Surf. Coat. Technol.*, 2017, **318**, p 365-373
  11. D.Y. Li, X.Y. Chen, X.D. Hui, J.P. Wang, P.P. Jin, and H. Li, Effect of Amorphicity of HVOF Sprayed Fe-Based Coatings on Their Corrosion Performances and Contacting Osteoblast Behavior, *Surf. Coat. Technol.*, 2017, **310**, p 207-213
  12. J.E. Berger, R. Schulz, S. Savoie, J. Gallego, C.S. Kiminami, C. Bolfarini, and W.J. Botta, Wear and Corrosion Properties of HVOF Coatings from Superduplex Alloy Modified with Addition of Boron, *Surf. Coat. Technol.*, 2017, **309**, p 911-919
  13. J.W. Li, L.J. Yang, H.R. Ma, K.M. Jiang, C.T. Chang, J.Q. Wang, Z.L. Song, X.M. Wang, and R.W. Li, Improved Corrosion Resistance of Novel Fe-Based Amorphous Alloys, *Mater. Des.*, 2016, **95**, p 225-230
  14. H.R. Ma, X.Y. Chen, J.W. Li, C.T. Chang, G. Wang, H. Li, X.M. Wang, and R.W. Li, Fe-Based Amorphous Coatings with High Corrosion and Wear Resistance, *Surf. Eng.*, 2017, **33**, p 56-62
  15. H.R. Ma, J.W. Li, J. Jiao, C.T. Chang, G. Wang, J. Shen, X.M. Wang, and R.W. Li, Wear Resistance of Fe-Based Amorphous Coatings Prepared by AC-HVOF and HVOF, *Mater. Sci. Technol.*, 2017, **33**, p 65-71
  16. Z. Zhou, L. Wang, D.Y. He, F.C. Wang, and Y.B. Liu, Microstructure and Electrochemical Behavior of Fe-Based Amorphous Metallic Coatings Fabricated by Atmospheric Plasma Spraying, *J. Therm. Spray. Technol.*, 2011, **20**, p 344-350
  17. K. Hashimoto, What We Have Learned from Studies on Chemical Properties of Amorphous Alloys, *Appl. Surf. Sci.*, 2011, **257**, p 8141-8150
  18. D.P. Wang, S.L. Wang, and J.Q. Wang, Relationship Between Amorphous Structure and Corrosion Behaviour in a Zr-Ni Metallic Glass, *Corros. Sci.*, 2012, **59**, p 88-95
  19. M.L. Morrison, R.A. Buchanan, A. Peker, P.K. Liaw, and J.A. Horton, Electrochemical Behavior of a Ti-Based Bulk Metallic Glass, *J. Non-Cryst. Solids*, 2007, **353**, p 2115-2124
  20. M. Metikoš-Huković, J. Katić, and I. Milošev, Kinetics of Passivity of NiTi in an Acidic Solution and the Spectroscopic Characterization of Passive Films, *J. Solid State Electrochem.*, 2012, **16**, p 2503-2513
  21. Y. Wang, S.L. Jiang, Y.G. Zheng, W. Ke, W.H. Sun, and J.Q. Wang, Electrochemical Behaviour of Fe-Based Metallic Glasses in Acidic and Neutral Solutions, *Corros. Sci.*, 2012, **63**, p 159-173
  22. Z.M. Wang, J. Zhang, X.C. Chang, W.L. Hou, and J.Q. Wang, Structure Inhibited Pit Initiation in a Ni-Nb Metallic Glass, *Corros. Sci.*, 2010, **52**, p 1342-1350
  23. Z. Li, C. Zhang, and L. Liu, Wear Behavior and Corrosion Properties of Fe-Based Thin Film Metallic Glasses, *J. Alloys Compd.*, 2015, **650**, p 127-135
  24. H. Luo, C.F. Dong, K. Xiao, and X.G. Li, Characterization of Passive Film on 2205 Duplex Stainless Steel in Sodium Thio-sulphate Solution, *Appl. Surf. Sci.*, 2011, **258**, p 631-639
  25. J. Xu, H.J. Huang, Z.Y. Li, S. Xu, H.L. Tao, P. Munroe, and Z.H. Xie, Corrosion Behavior of a ZrCN Coated Ti Alloy with Potential Application as a Bipolar Plate for Proton Exchange Membrane Fuel Cell, *J. Alloys Compd.*, 2016, **663**, p 718-730
  26. M. Sowa, D. Łastówka, A.I. Kukhareenko, D.M. Korotin, E.Z. Kurmaev, S.O. Cholakh, and W. Simka, Characterisation of Anodic Oxide Films on Zirconium Formed in Sulphuric Acid: XPS and Corrosion Resistance Investigations, *J. Solid State Electrochem.*, 2017, **21**, p 203-210
  27. M.A. Rodriguez and R.M. Carranza, Properties of the Passive Film on Alloy 22 in Chloride Solutions Obtained by Electrochemical Impedance, *J. Electrochem. Soc.*, 2011, **158**, p C221-C230
  28. D.D. Macdonald, The Point-Defect Model for the Passive State, *J. Electrochem. Soc.*, 1992, **139**, p 3434-3449
  29. D.D. Macdonald, On the Existence of Our Metals-Based Civilization I. Phase-Space Analysis, *J. Electrochem. Soc.*, 2006, **153**, p B213-B224
  30. M.G.S. Ferreira, M.D.C. Belo, N.E. Hakiki, G. Goodlet, M.F. Montemor, and A.M.P. Simões, Semiconducting Properties of Oxide and Passive Films Formed on AISI, 304 Stainless Steel and Alloy 600, *J. Braz. Chem. Soc.*, 2002, **13**, p 433-440
  31. Y. Yang, X.H. Ning, H.S. Tang, L.J. Guo, and H.T. Liu, Effects of Passive Films on Corrosion Resistance of Uncoated SS316L bipolar Plates for Proton Exchange Membrane Fuel Cell Application, *Appl. Surf. Sci.*, 2014, **320**, p 274-280
  32. T. Yamamoto, K. Fushimi, H. Habazaki, and H. Konno, Depassivation-Repassivation Behavior of a Pure Iron Surface Investigated by Micro-indentation, *Electrochim. Acta*, 2010, **55**, p 1232-1238
  33. S.J. Ahn and H.S. Kwon, Effects of Solution Temperature on Electronic Properties of Passive Film Formed on Fe in pH 8.5 Borate Buffer Solution, *Electrochim. Acta*, 2004, **49**, p 3347-3353
  34. J.R. Scully, A. Gebert, and J.H. Payer, Corrosion and Related Mechanical Properties of Bulk Metallic Glasses, *J. Mater. Res.*, 2007, **22**, p 302-313
  35. M. Zhou, K. Hagos, H.Z. Huang, M. Yang, and L.Q. Ma, Improved Mechanical Properties and Pitting Corrosion Resistance of Zr<sub>65</sub>Cu<sub>17.5</sub>Fe<sub>10</sub>Al<sub>7.5</sub> Bulk Metallic Glass by Isothermal Annealing, *J. Non-Cryst. Solids*, 2016, **452**, p 50-56
  36. M. Ghahari, D. Krouse, N. Laycock, T. Rayment, C. Padovani, M. Stampanoni, F. Marone, R. Mokso, and A.J. Davenport, Synchrotron X-Ray Radiography Studies of Pitting Corrosion of Stainless Steel: Extraction of Pit Propagation Parameters, *Corros. Sci.*, 2015, **100**, p 23-35
  37. C. Luo, S.P. Albu, X.R. Zhou, Z.H. Sun, X.Y. Zhang, Z.H. Tang, and G.E. Thompson, Continuous and Discontinuous Localized Corrosion of a 2xxx Aluminium-Copper-Lithium Alloy in Sodium Chloride Solution, *J. Alloys Compd.*, 2016, **658**, p 61-70
  38. J.A. Hammons, A.J. Davenport, S.M. Ghahari, M. Monir, J.P. Tinnes, M. Amri, N. Terrill, F. Marone, R. Mokso, M. Stampanoni, and T. Rayment, Interfacial Phenomena During Salt Layer Formation Under High Rate Dissolution Conditions, *J. Phys. Chem. B*, 2013, **117**, p 6724-6732
  39. R.A. Bley, J.R. Scully, and J.W.P. Hsu, Microstructure Dependence of Nanometre Corrosion in Al-Ni-Y Glassy Alloys, *Philos. Mag. Lett.*, 2000, **80**, p 85-94